Horizon Multidisciplinary Scientific Journal
Journal homepage: https://horizonmsj.com/

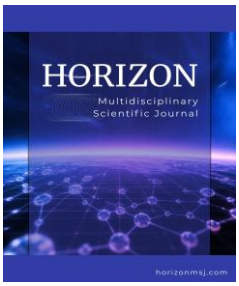

Original Research Paper

Structural and Thermal Characterization of Boron-Doped Nano TiO_2: Hydrothermal Synthesis for Flame-Retardant Nanomaterials

Huseyn Imanov
https://orcid.org/0000-0002-6970-5645

[1]*Faculty of Natural Sciences and Agriculture, Department of Chemistry, Nakhchivan State University, Nakhchivan, Azerbaijan*

Article history
Received: 17.03.2026
Revised: 28.03.2026
Accepted: 02.04.2026

*Corresponding Author: Huseyn Imanov, Faculty of Natural Sciences and Agriculture, Department of Chemistry, Nakhchivan State University, Nakhchivan, Azerbaijan;
Email: huseyn.imanov@ndu.edu.az

Abstract
In this study, the structural, morphological, and thermal effects of doping nano-sized titanium dioxide (TiO_2) with two distinct boron sources—boron oxide (B_2O_3) and boric acid (H_3BO_3)—were systematically investigated. Synthesis was performed via the hydrothermal method in a PTFE-lined autoclave reactor at 200 °C for 4 hours. Comprehensive characterization of the resulting nanomaterials was conducted using X-ray diffraction (XRD), scanning electron microscopy (SEM), energy dispersive X-ray spectroscopy (EDS), and thermogravimetric/differential scanning calorimetry (TGA/DSC) analysis. XRD results confirmed that the TiO_2 matrix retained its anatase crystal structure in both doping approaches. SEM images revealed grain sizes in the range of 96–97 nm for boron oxide-doped samples and 96–111 nm for boric acid-doped samples. EDS confirmed the successful integration of dopant elements (B, O, Ti) into the structure. TGA/DSC data verified endothermic phase transitions at ~228 °C for B_2O_3-doped samples and below 200 °C for H_3BO_3-doped samples, fully consistent with the B_2O_3–H_2O phase diagram. The findings demonstrate that boron doping renders TiO_2 nanostructures a promising material for flame-retardant textile applications.

Keywords: *Nano TiO_2, Boron Doping, Hydrothermal Synthesis, Anatase, Flame Retardancy, Thermal Characterization, XRD, SEM*

1. INTRODUCTION

Titanium dioxide (TiO_2) is one of the most extensively investigated semiconducting metal oxides in the fields of environmental remediation, energy conversion, and advanced materials science, owing to its outstanding photocatalytic activity, high chemical stability, low toxicity, and cost-effectiveness [1–3]. TiO_2 exists in three primary polymorphic crystal structures—anatase, rutile, and brookite—among which the anatase form is of particular significance due to its superior photocatalytic performance, making it highly relevant for photovoltaic systems, photocatalysts, and self-cleaning surfaces [4,5, 23].

DOI: https://doi.org/10.5281/zenodo.19665545

Nevertheless, the relatively wide bandgap of TiO_2, approximately 3.0–3.2 eV, limits its ability to utilize the visible light spectrum efficiently, thereby constraining its practical applications [6]. To overcome this limitation, a variety of cationic and anionic doping strategies have been developed within the framework of bandgap engineering. The incorporation of non-metals such as nitrogen (N), sulfur (S), phosphorus (P), and boron (B), as well as transition metal ions including Fe3+, Cu2+, and Zn2+, into the TiO_2 lattice can profoundly transform its electronic and surface properties [7,8].

Boron doping is regarded as a particularly attractive approach for TiO_2 modification, primarily because boron can be incorporated into the TiO_2 lattice in both cationic (B^{3+}) and anionic (B^{3-}) forms, simultaneously improving surface acidity, photocatalytic efficiency, and thermal stability. Furthermore, boron oxide (B_2O_3) is a well-established flame retardant compound, particularly in the textile industry [9,10].

This study presents a comprehensive structural, morphological, and thermal characterization of boron-doped nano TiO_2 materials synthesized via the hydrothermal method using two different boron precursors: B_2O_3 and H_3BO_3. The principal original contribution of this work is the systematic comparison of the effects of these two boron sources—differing in their phase states—on the crystal structure, grain morphology, and thermal behavior of the doped product. The resulting nanomaterials are evaluated as candidates for flame-retardant textile applications, leveraging the flame-inhibiting function of the boron oxide content.

2. THEORETICAL BACKGROUND AND LITERATURE REVIEW

2.1. Crystal Structure and Photocatalytic Significance of TiO_2

TiO_2 occurs in three polymorphic forms: anatase, rutile, and brookite. Anatase and rutile adopt tetragonal symmetry, while brookite is orthorhombic. The fundamental structural unit in all polymorphs is the TiO_6 octahedron; however, differences in octahedral connectivity give rise to the distinct physicochemical properties characteristic of each phase [5]. The anatase phase exhibits the highest photocatalytic activity, attributed to its bandgap of approximately 3.2 eV, high electron mobility, and superior surface area. Upon calcination in the range of 660–950 °C, anatase undergoes an irreversible transformation to the thermodynamically stable rutile phase [5]. Rutile (3.0 eV) offers advantages in visible light absorption, yet its photocatalytic activity remains lower than that of anatase. Hydrothermal synthesis, which enables direct control over grain size, surface area, and phase composition, has emerged as a versatile method capable of producing all three polymorphs [11].

2.2. Chemistry of Boron Compounds and Their Role in TiO_2 Doping

The thermal dehydration of boric acid (H_3BO_3) proceeds through a stepwise phase transformation, initially forming metaboric acid (HBO_2) and subsequently yielding fully dehydrated boron oxide (B_2O_3).

DOI: https://doi.org/10.5281/zenodo.19665545

The B_2O_3–H_2O phase diagram precisely defines the boundary conditions of these transformations: H_3BO_3 is stable up to approximately 170 °C, and HBO_2 remains stable between 176 °C and 236 °C [20]. These phase transitions directly influence the properties of the final product depending on the boron source employed during doping.

The incorporation of boron into the TiO_2 lattice can occur via two competing mechanisms: (i) substitutional doping, in which B^{3+} ions occupy titanium sites, and (ii) interstitial doping, in which B3+ ions fill oxygen vacancies. Both mechanisms introduce oxygen vacancies into the TiO_2 structure, enhancing photoabsorption capacity and thereby increasing photocatalytic activity under visible light [9,10]. Moreover, residual boron oxide phases at the surface are known to exhibit flame-retardant behavior, creating potential application opportunities in the textile industry through their interaction mechanism with cotton fibers.

2.3. Hydrothermal Synthesis Method

Hydrothermal synthesis refers to the crystal growth process carried out in aqueous solution under elevated temperature and pressure conditions. Typically conducted in autoclaves at temperatures ranging from 100 to 374 °C and pressures of 1–500 MPa, this approach offers several advantages for nanomaterial synthesis: precise control over grain size and morphology, narrow size distribution, high purity, and the direct production of nanometric products without the need for additional calcination steps [11]. Compared to the sol-gel method, hydrothermal synthesis enables homogeneous nucleation and controlled growth conditions, as the product forms directly within the solution medium [12-19, 21].

3. MATERIALS AND METHODS

3.1. Chemicals and Reagents

Tetrapropyl orthotitanate (Ti(OPr*n*)$_4$) was used as the titanium precursor, isopropyl alcohol (IPA) as the solvent, and analytical-grade boron oxide (B_2O_3) and boric acid (H_3BO_3) as the boron sources. All reagents were used as received without further purification.

3.2. Hydrothermal Synthesis Procedure

The synthesis was carried out under standardized conditions with a water-to-alkoxide molar ratio of 3.0 and pH 5.5. The titanium precursor (42.47 mL of tetrapropyl orthotitanate, equivalent to 40 g of Ti) was first dissolved in 97.73 mL of IPA and homogenized under magnetic stirring for 15 minutes. Subsequently, 0.2 g of either B_2O_3 or H_3BO_3 was dissolved using a combination of magnetic stirring and ultrasonic bath, then added dropwise to the main solution via burette and stirred for an additional 15 minutes. A water-IPA mixture (27.92 mL IPA + 6.48 mL H_2O) was then added in the same dropwise manner, and the resulting mixture was stirred continuously for 30 minutes.

DOI: https://doi.org/10.5281/zenodo.19665545

The prepared solution was transferred to PTFE-lined autoclave reactors and subjected to hydrothermal reaction at 200 °C for 4 hours. After the reaction, the system was left sealed for 24 hours to allow natural cooling to room temperature. The resulting solid precipitate was filtered using a No. 4 pore filter and vacuum pump assembly, washed thoroughly with pure ethanol followed by deionized water, and then dried in a vacuum oven at 75 °C for 48 hours. The dried products were ground into powder and stored for further characterization.

3.3. Characterization Techniques

X-ray diffraction (XRD) analysis was performed using CuKα radiation (λ = 1.54 Å) at 40 kV and 40 mA, over a 2θ scanning range of 5°–70° with a step size of 0.02°/step [22]. Phase identification was carried out with reference to the JCPDS database compiled by the ICDD. Crystallite size was calculated using the Scherrer equation ($D = K\lambda/\beta\cos\theta$). Morphological investigations were conducted using a JEOL JSM-5910LV scanning electron microscope (SEM) at an accelerating voltage of 20 kV and magnifications of 10,000× and 50,000×. Elemental composition was determined by energy dispersive X-ray spectroscopy (EDS) integrated into the same instrument. Thermal characterization was performed using an SDT Q600 simultaneous DSC-TGA instrument from room temperature to 1000 °C at a heating rate of 10 °C/min under a nitrogen atmosphere.

4. RESULTS AND DISCUSSION

4.1. X-Ray Diffraction (XRD) Analysis

The XRD patterns of both doped samples exhibit intense and well-defined anatase TiO_2 diffraction peaks. In the boron oxide-doped sample, the most intense peaks at 25.36° and 27.70° 2θ correspond to anatase TiO_2 (JCPDS 21-1272) and the B_2O_3 phase, respectively. In the boric acid-doped sample, strong peaks at 25.32° and 26.17° 2θ similarly indicate the anatase phase alongside residual H_3BO_3/B_2O_3 phases. The preservation of the anatase structure in both samples confirms that the hydrothermal synthesis conditions and the doping concentration were carefully optimized to prevent phase transformation to rutile.

A notable broadening of XRD peaks was observed in the boric acid-doped sample compared to the boron oxide-doped one. Based on the Scherrer equation, peak broadening is directly related to a reduction in crystallite size. This finding suggests that the use of H_3BO_3 promotes the formation of finer crystalline domains compared to B_2O_3. This difference can be attributed to the distinct solubility and reactivity of the two precursors: H_3BO_3 exhibits higher solubility under hydrothermal conditions, providing a more homogeneous nucleation environment.

4.2. Morphological Analysis (SEM)

SEM images reveal a compact morphology consisting of equiaxed, agglomerated nanoparticles in both samples. In the B_2O_3-doped TiO_2 sample, grain sizes measured at 50,000× magnification fall within

DOI: https://doi.org/10.5281/zenodo.19665545

the range of 96–97 nm, indicating an exceptionally narrow size distribution. In the H_3BO_3-doped sample, grain sizes were measured in the range of 96–111 nm, reflecting a comparatively broader size distribution. The fact that grain sizes in both samples remain at or below 100 nm confirms the successful preservation of nanoscale architecture throughout the synthesis process.

The observed differences in grain size can be explained by the distinct thermal reactivity of the two boron sources. B_2O_3 adopts a glass-like viscous state at elevated temperatures and may act as a growth-inhibiting barrier by coating the TiO_2 grain surfaces, thereby accounting for the more uniform size distribution observed. H_3BO_3, on the other hand, generates active boron species under hydrothermal conditions that interact with both the surrounding medium and the TiO_2 surface, leading to a partially different nucleation and growth kinetics.

4.3. Elemental Composition (EDS) Analysis

EDS analysis confirmed the presence of Ti, O, and B in both samples. In the B_2O_3-doped sample, the elemental composition was determined as B: 19.01 wt.%, O: 39.37 wt.%, and Ti: 41.62 wt.%. In the H_3BO_3-doped sample, the corresponding values were B: 20.83 wt.%, O: 41.73 wt.%, and Ti: 37.44 wt.%. These results confirm that the dopant boron element was successfully integrated into the synthesized nano TiO_2 structure in both approaches.

Notably, the H_3BO_3-doped sample exhibited a higher boron content (20.83 wt.%) alongside a lower Ti proportion (37.44 wt.%) compared to the B_2O_3-doped sample (Ti: 41.62 wt.%). This observation suggests that the higher solubility of the H_3BO_3 precursor facilitated a greater incorporation of boron into the TiO_2 matrix. In both samples, the O/Ti ratio exceeds the expected stoichiometry, pointing to the presence of residual boron oxide phases—an observation consistent with the XRD findings.

4.4. Thermal Analysis (TGA/DSC) Results

TGA/DSC analyses provide one of the most critical findings confirming the hypothesis of this study. A pronounced endothermic event was observed at 228.29 °C in the B_2O_3-doped sample. This temperature coincides with the stability boundary of the B_2O_3 phase in the B_2O_3–H_2O phase diagram, confirming that the boron oxide component within the product exhibits the predicted thermal behavior. In contrast, the endothermic transformation occurring below 200 °C in the H_3BO_3-doped sample corresponds to the conversion of H_3BO_3 to metaboric acid (HBO_2), which is in full agreement with the H_3BO_3 decomposition region in the phase diagram.

Both samples exhibited an initial mass loss of approximately 5–10 wt.% attributable to the removal of adsorbed water and surface hydroxyl groups, with the majority of this weight loss completed below 400 °C. This defines the appropriate pre-sintering heat treatment temperature range, which is of practical significance. The negligible weight change observed at higher temperatures confirms the preservation of the thermal stability of the TiO_2 matrix. Collectively, these findings demonstrate that both boron sources

DOI: https://doi.org/10.5281/zenodo.19665545

were successfully integrated into the TiO_2 structure while retaining their characteristic phase transition kinetics.

4.5. Comparative Assessment of Doping Mechanisms

When the findings are evaluated as a whole, the two boron sources appear to operate through distinct doping mechanisms. The B_2O_3-doped samples are characterized by a narrower grain size distribution, lower boron content, and a thermal transition near 228 °C. Structurally, B_2O_3 is thought to predominantly reside at grain boundaries, forming a coating over TiO_2 particles. The H_3BO_3-doped samples, by contrast, are distinguished by a broader grain size distribution, higher boron content, and a thermal transition below 200 °C. Given the higher solubility of H_3BO_3, it is anticipated that boron is incorporated largely into the TiO_2 lattice or forms a very thin interfacial layer.

A noteworthy observation is the preservation of the anatase structure in both approaches, despite the use of different boron sources and markedly different synthesis mechanisms. This indicates that the hydrothermal synthesis conditions (0.5 wt.% doping ratio, pH 5.5, 200 °C) exert a dominant influence on the stability of the anatase phase. Scherrer crystallite sizes calculated from XRD and SEM measurements are in good agreement, suggesting that the particles exist as single crystals or units composed of a small number of crystallites.

5. CONCLUSION

In this study, boron-doped nano TiO_2 materials synthesized via the hydrothermal method using B_2O_3 and H_3BO_3 were comprehensively characterized by XRD, SEM, EDS, and TGA/DSC techniques. The principal findings and overall conclusions of the study are summarized below:

1. XRD analysis confirmed the preservation of the anatase crystal structure of the TiO_2 matrix in both doping approaches, demonstrating that the selected hydrothermal synthesis conditions (200 °C, pH 5.5, water-to-alkoxide ratio = 3.0) are highly suitable for maintaining anatase phase stability.
2. SEM analysis confirmed the formation of genuine nano-scale grain structures in the range of 96–97 nm for B_2O_3-doped samples and 96–111 nm for H_3BO_3-doped samples. The B_2O_3 source was found to exert a more pronounced inhibitory effect on grain growth.
3. EDS characterization verified the successful incorporation of the dopant boron element into the TiO_2 structure in both samples, with the H_3BO_3 source enabling a higher degree of boron incorporation due to its greater solubility.
4. TGA/DSC analyses clearly distinguished the divergent thermal behaviors of the two boron sources: the endothermic transitions at 228 °C for B_2O_3-doped samples and below 200 °C for H_3BO_3-doped samples are in full agreement with the B_2O_3–H_2O phase diagram, confirming that boron sources in different phase states significantly influence the thermal stability of the final product.

DOI: https://doi.org/10.5281/zenodo.19665545

5. Both precursors were shown to enable the successful synthesis of boron-containing nano TiO_2 materials: the B_2O_3 source yields a narrow size distribution, while the H_3BO_3 source provides a higher boron content—allowing precursor selection to be tailored to the requirements of the intended application.
6. The boron oxide component within the nano TiO_2 structure is considered to possess flame-retardant potential through bonding to textile fibers, positioning the resulting materials as promising candidates for functional textile applications.

Future research directions should focus on the systematic variation of boron doping concentration and evaluation of photocatalytic activity under visible light irradiation, elucidation of the boron cation/anion equilibrium mechanism via XPS analysis, and assessment of the practical flame-retardant performance of the synthesized nanomaterials in textile systems.

REFERENCES

[1] Fujishima, A., Honda, K. (1972). Electrochemical photolysis of water at a semiconductor electrode. Nature, 238(5358), 37–38.

[2] Linsebigler, A.L., Lu, G., Yates, J.T. (1995). Photocatalysis on TiO_2 surfaces: principles, mechanisms, and selected results. Chemical Reviews, 95(3), 735–758.

[3] Chen, X., Mao, S.S. (2007). Titanium dioxide nanomaterials: synthesis, properties, modifications, and applications. Chemical Reviews, 107(7), 2891–2959.

[4] Hanaor, D.A.H., Sorrell, C.C. (2011). Review of the anatase to rutile phase transformation. Journal of Materials Science, 46(4), 855–874.

[5] Bhave, R.C., Lee, B.I. (2007). Experimental variables in the synthesis of brookite phase TiO_2 nanoparticles. Materials Science and Engineering A, 467(1–2), 146–149.

[6] Asahi, R., Morikawa, T., Ohwaki, T., Aoki, K., Taga, Y. (2001). Visible-light photocatalysis in nitrogen-doped titanium oxides. Science, 293(5528), 269–271.

[7] Zhao, W., Ma, W., Chen, C., Zhao, J., Shuai, Z. (2004). Efficient degradation of toxic organic pollutants with Ni_2O_3/TiO_2xBx under visible irradiation. Journal of the American Chemical Society, 126(15), 4782–4783.

[8] In, S., Orlov, A., Berg, R., García, F., Pedrosa-Jimenez, S., Tikhov, M.S., Armstrong, D., Lambert, R.M. (2007). Effective visible light-activated B-doped and B,N-codoped TiO_2 photocatalysts. Journal of the American Chemical Society, 129(45), 13790–13791.

[9] Liu, G., Zhao, Y., Sun, C., Li, F., Lu, G.Q., Cheng, H.M. (2008). Synergistic effects of B/N doping on the visible-light photocatalytic activity of mesoporous TiO_2. Angewandte Chemie International Edition, 47(24), 4516–4520.

[10] Finnie, K.S., Bartlett, J.R., Woolfrey, J.L. (1999). Boron-containing titania sol–gel films: effect of B_2O_3 on crystallisation. Journal of Materials Chemistry, 9(7), 1681–1685.

[11] Yoshimura, M., Byrappa, K. (2008). Hydrothermal processing of materials: past, present and future. Journal of Materials Science, 43(7), 2085–2103.

[12] Imanov, H., Jafarli, M., Mahmudov, S., & Karimova, S. (2025). Investigation of the Conditions for Obtaining the Silver Thioarsenate Compound from the $AgNO_3$-As_2S_5-H_2O System and Investigation of the Properties of the Obtained Silver Thioarsenate Compound. 1600-1612.

[13] Imanov, H., & Jafarli, M. (2025). Investigation of the interaction conditions of As_2S_5 and $CuCl_2$ compounds in water and ethylene glycol medium. Turkish Journal of Chemistry, 49(2), 204-214.

[14] Imanov, H., & Huseynov, Q. (2021). Investigation of the Acquisition Conditions of Tl_3AsS_4 Compound in the Aquatic Environment. Journal of the Turkish Chemical Society Section A: Chemistry, 8(2), 527-534.

[15] Imanov, H., & Huseynov, Q. (2020). Investigation of acquisition of triple sulfurs from $Pb(CH_3COO)_2$-Na_3AsO_4-H_2S-H_2O system by hydrochemical method. Journal of the Turkish Chemical Society Section B: Chemical Engineering, 3(2), 35-40.

[16] Imanov, H. A., & Huseynov, G. M. (2021). Study of the conditions for the acquisition of Tl_3AsS_4 in ethylene glycol. Kimya Problemleri, (3), 135-142.

[17] Əliyeva S.H., Hüseynov Q.M. (03-06 Mart 2020). Hidrokimyəvi metodla Tl_3SbS_4 birləşməsinin alınması // Seconda İnternational Scientific Conference of Young Scientists and Specialist SOCAR, p.315-317.

[18] Hüseynov Q.M., Əliyeva S.H. (2020). Hidrotermal şəraitdə $TlSb^{+3}(Sb^{+5})S^{-2}$-H_2O sistemlərindən üçlü sulfidlərin alınması. Naxçıvan: AMEA Naxçıvan Bölməsi Elmi Əsərlər, Təbiət və Texniki Elmlər seriyası. 4, s.30-36.

[19] Алиева С.Н. (2024). Исследование Условий Получения Тиостибиата Серебра(I) из системы Sb_2S_5-$AgNO_3$-H_2O. Международный научный журнал «Наука и Мир» Volgograd. 7 cild 131, с.20-26

[20] Adams, R.M. (1964). Boron, Metallo-Boron Compounds and Boranes. Interscience Publishers, New York.

[21] Venkatachalam, N. et al. (2007). Sol-gel preparation and characterization of nanosize TiO_2. Materials Chemistry and Physics, 104(2–3), 454–459.

[22] Scherrer, P. (1918). Bestimmung der Größe und inneren Struktur von Kolloidteilchen mittels Röntgenstrahlen. Nachrichten von der Gesellschaft der Wissenschaften zu Göttingen, 2, 98–100.

[23] Matthews, R.W. (1993). Photocatalytic purification and treatment of water and air. In: Ollis, D.F., Al-Ekabi, H. (Eds.), Elsevier, Amsterdam.